Thermal Science and Engineering Progress 37 (2023) 101616

Contents lists available at ScienceDirect

Thermal Science and Engineering Progress

journal homepage: www.sciencedirect.com/journal/thermal-science-and-engineering-progress

Hydrothermal performance of inline and staggered arrangements of airfoil shaped pin-fin heat sinks: A comparative study

Hamza Babar [a], Hongwei Wu [a,*], Hafiz Muhammad Ali [b,c,*], Wenbin Zhang [d]

[a] School of Physics, Engineering and Computer Science, University of Hertfordshire, Hatfield AL10 9AB, United Kingdom
[b] Mechanical Engineering Department, King Fahd University of Petroleum & Minerals (KFUPM), Dhahran 31261, Saudi Arabia
[c] Interdisciplinary Research Center for Renewable Energy and Power Systems (IRC-REPS), King Fahd University of Petroleum and Minerals, Dhahran 31261, Saudi Arabia
[d] School of Science and Technology, Nottingham Trent University, Clifton Lane, Nottingham NG11 8NS, United Kingdom

ARTICLE INFO

Keywords:
Heat sink
Thermal management
Airfoil
Electronic cooling
Hydrothermal performance

ABSTRACT

The distinctive airfoil shaped pin-fins offer minimal resistance to fluid flow and enormous effective area due to the delayed fluid separation at the tail. In this article, the hydrothermal performance of inline and staggered arrangement of airfoil pin-fins heat sink for electronic systems was experimentally evaluated in a systematic manner. The comparative study was carried out by varying the Reynolds number and heating power ranging from 600 to 860 and 75 W to 125 W, respectively. To ensure the same surface area, the number of pin fins was identical in both configurations. Nusselt number, thermal resistance, pumping power, and overall performance were the examined parameters. Interestingly, the Nusselt number for inline arrangement of pin fins was observed to be higher, while the overall performance of the staggered configuration was revealed to be better. This could be caused by the increased pressure drop in the inline arrangement of pin fins. Experimental results revealed that the Nusselt number for inline configuration was almost 3.96 % higher than staggered arrangement at the highest heating power. In addition, the penalty of pumping power was also observed to be more for inline configuration. It was noted that to pump fluid at the same rate, an average of approximately 2.93 % more power would be required for inline geometry. A significant improvement in heat transfer was observed with a substantial drop in pumping power while increasing the heating power. Finally, the overall performance was examined, revealing that the staggered arrangement delivered better results. In comparison, a maximum of 1.81 % improvement in overall performance for staggered geometry was determined at 75 W, which reduced as heating power increased.

1. Introduction

Recent advances in the electronics industry have exacerbated the cooling problem due to the incorporation of compact systems that generate exorbitant heat. Data centers consumes 1.31 % of total electricity globally with thermal management accounts for 33 % [1]. For every 2 °C increase in temperature, it was revealed that the reliability of silicon chips decreased by about 10 %. The temperature rise is the major cause of electronic components failure which accounts for 55 % compared to the other factors like vibration, humidity, and dust, each of which accounts for 20 %, 19 %, and 6 %, respectively [2]. The reliability concerns with electronic systems are urging investigators to shift towards liquid colling techniques away from air cooling. Single-phase cooling has proven to be very effective for thermal management of high heat generating chips [3,4]. Most of the studies conducted on heat sinks have focused on reducing the core temperature improving heat transfer. However, it is also crucial to keep the pressure drop to a minimal, resulting in a low pumping power requirement. Along with the rate of heat transfer, the pressure drop is also a significant factor that needs to be considered to develop an optimum design of the heat sink. Nowadays various geometrical configurations of heat sinks have been examined [5,6]. It was revealed that with a considerable improvement in heat transfer pressure drop elevated significantly as the fins resist fluid flow. Thus, a slight increase in heat transfer at the expense of excessive pumping power is undesirable. To augment the rate of heat transfer, the optimization of sink design plays a very significant role. Xie et al. [7] studied the influence of fins length on pressure drop and heat transfer rate in the laminar flow regime. It was observed that the overall thermal performance augmented with an increase in fin length and the

* Corresponding authors.
E-mail addresses: h.babar@herts.ac.uk (H. Babar), h.wu6@herts.ac.uk (H. Wu), hafiz.ali@kfupm.edu.sa (H.M. Ali), wenbin.zhang@ntu.ac.uk (W. Zhang).

https://doi.org/10.1016/j.tsep.2022.101616
Received 20 August 2022; Received in revised form 5 December 2022; Accepted 9 December 2022
Available online 12 December 2022

Nomenclature

CNC	Computer Numerical Control
HTC	Heat transfer coefficient
LFR	Laminar flow regime
LMTD	Logarithmic mean temperature difference
MRE	Mean reletive error
MCHS	Mini channel heat sink
PD	Pressure drop
PP	Pumping power

Symbols

A	Surface area [m^2]
AR	Aspect ratio
$A_{s,top}$	Top surface area of fin [m^2]
A_w	Wetted area [m^2]
c_p	Heat capacity [J/kg °C]
D	Diameter [m]
d_h	Hydraulic diameter [m]
f	Friction factor
h	Heat transfer coefficient [W/m^2 °C]
k	Thermal conductivity [W/m °C]
L	Length [m]
L_{fin}	Length of fin [m]
M	Molecular weight
m	Mass [kg]
$\dot{m}$	Mass flow rate [kg/s]
N	Avogadro's number
n	fins number of rows
ΔP	Pressure drop [bar]
Pr	Prandtl number
P_{fin}	Perimeter of fin [m]
Q	Heat transfer rate [W]
R_{th}	Thermal *Res*istance [m^2 °C/W]
Re	Reynolds number
T	Temperature [°C]
$U_{exp.}$	Experimental quantity
U_{ss}	Volume of sepecific section
$U_{pred.}$	Predicted quantity
V	Volumetric flow rate
v	Fluid velocity
W	Width [m]

Greek letter

ρ	Density [kg/m^3]
μ	Viscosity [kg/mÂ·s]

Subscript

b	base
eff	Effective
f	Fin
m	mean
s	Heat sink
s	Specific section
w	Wall

heat transfer capacity of finned surfaces was significantly higher than that of flat surfaces. Their results revealed that obstacles disrupt the boundary layer and boundary layer destroyed and rebuilt across the fins, causing the increase in heat transfer rate. Chai et al. [8] comprehensively studied the effect of different shaped fins (rectangular, elliptical, diamond, and triangular) in the interrupted micro channels. Their study was conducted in the laminar flow regime exhibited that elliptical fins in combination with interrupted channels delivered the best thermal performance compared to other fins. The maximum enhancement of 57 % and 70 % was noticed for Nusselt number and friction factor over straight channels, respectively. Wu et al. [9] examined the novel tree-shaped heat sink for the systems that generate heat in the range of 5–8 W/cm^2. The designed heat sink was deemed to be effective since the surface temperature never exceeded 66.6 °C at peak heating value. The layered heat sinks are currently in discussion for better thermal characteristics. According to Hong et al. [10], the double-layered channel structure is ineffective for increasing energy efficiency. The coolant temperature rose significantly after flowing through the first layer, the amount of pressure loss is almost identical in second layer while having a substantially lower cooling capacity.

Hung et al. [11] investigated the thermal and hydraulic performance of mini-channel heat sink (MCHS) made of porous copper with various channel configurations. The parameters such as heat transfer coefficient (HTC) and pumping power observed against the Reynolds numbers in the laminar regime (45–1350). Their analysis stated that the porous media could improve the thermal performance, while a significant improvement was also noted with the increase in Reynolds number. It was observed that the sandwich distribution of porous medium performed well thermally and hydraulically among the investigated configurations. Tullius et al. [12] compiled a study to investigate the effect of several aspects such as pin fin shape, materials, spacing, and width. Investigators inspected the impact of six different pin fins shapes (hexagon, ellipse, triangle, square, diamond, circle) and four different materials (aluminium, CNT, copper, and silicon) on heat transfer characteristics and pressure drop with varying the inlet velocity and heat flux. It was concluded that the plate with triangular fins could provide the highest Nusselt number while the pressure drop was minimum with the circular and ellipse shaped pin fins. However, both the Nusselt number and pressure drop augmented with the increase in fin height, spacing and width. Jajja et al. [13] compared the thermal performance of MCHS with the flat plate sink varying fins spacing (0.1, 0.5, 1, 1.5 mm). The thermal resistance and base temperature were found to be reduced with an increase in flow rate. According to the results, thermal resistance was reduced from 0.216 K/W to 0.03 K/W with the addition of fins on the surface of sink. In addition, the HTC was enhanced from 1297 W/m^2·K to 2156 W/m^2·K using the sink of fin spacing 0.2 mm. The effectiveness of straight channel heat sinks introducing various butterfly insert configurations was explored by Sudheer and Madanan [14]. The results were inspected for each insert varying pitch and perforation in wings. Friction factor was found to be reduced significantly with perforated wings but with the penalty of considerable reduction in heat transfer. Considering overall thermal performance, sinks having unperforated inserts recommended over perforated inserts. This affirms that the sink performance cannot be determined solely by heat transfer. Tang et al. [15] experimentally inspected the cooling performance of heat sink varying the angle and depth of bio-inspired wave structure. The depth of the wave structure helped to intensify the heat transfer. The performance also improved with angle up to a certain point before it started to decline, lowest temperature was recorded at 65°.

The performance of inline and staggered arrangement of square pin-fin was experimentally examined by Ali and Arshad [16]. Their study was conducted in the laminar flow regime employing water and some advanced thermal coolants. They stated that the staggered configurations could offer better thermal characteristics in comparison of inline fins arrangement. For sharp edge square shaped fins, it was due to the interaction of more fluid with fins in staggered arrangement. The study by Yan et al. [17] on the finned heat sink concluded that the flow

splitting point was affected by the geometry of the fins and consequently effects the magnitude of the vortex at the trailing end of the fins. Maji et al. [18] examined the hydrothermal characteristics of fins with various shaped perforation such as diamond, elliptical, and circular. It was found that changing the fin shape from circular to elliptical could result in a significant increase in Nusselt number with a noticeable reduction in pressure drop. According to Cui et al. [19] the staggered arrangement and appropriate shape of fins could effectively reduce the boundary layer effect and optimize the hydrothermal performance.

These types of heat sinks have been developed for the cooling of electronic components like processors with the goal of dissipating the appropriate amount of heat with the least degree of pressure drop. In this study, the heating power varies in the range of 75 W–125 W considering the thermal design power of intel Xeon silver processors. Most of the silver category processors of intel Xeon family generates heat in the range being examined in the current experimental investigation.

The literature reports a considerable number of studies on airfoil shape applications in various areas [20–23]. There are very limited studies on airfoil shaped extended surfaces for cooling applications. The available studies examined this special shape considering critical CO_2, refrigerant (R-123), and air as a cooling agent [24–27]. To the best of the authors' knowledge, no experimental study has been reported on the hydrothermal performance of water based airfoil shaped pin-fin heat sink altering fin position for electronic components cooling. This study is significant due to the unique effect of airfoil pin-fins, for most of the geometrical configurations the staggered arrangement showed better thermal performance [16–18], but it is not the case for airfoil shape [25]. Restrictions or pin fins influence the heat transfer and fluid flow in two ways: increasing the surface area in contact with the flowing fluid and disrupting the flow. However, the plus point of airfoil pin fins is their minimal resistance to fluid flow. The prime focus of this study is to compare the performance of inline and staggered geometrical configurations considering thermal and hydraulic performance simultaneously.

2. Experimental setup

The closed loop experimental rig used during this experimental investigation was an interconnection of various components i.e. coolant storage tank, mini-hydraulic pump, needle value, micro-flowmeter, heat sink test section, radiator, and a pressure transducer. The schematic depiction of an entire loop with all linked equipment used to measure and record values is shown in Fig. 1. The cycle begins with the pump, which is in charge of pumping coolant from the storage tank. A needle vale was installed just after the pump to control and alter the flow of coolant. Prior to the coolant entered the heat sink section, a mounted flow meter measured the flow rate and displayed it on a digital display. The fluid flows through the channels and absorbs heat, lowering the temperature of the sink. Three cartridge heaters were positioned inside the heat sink to ensure a steady heat flux, while six thermocouples (5TC-TT-KI-24-2M, Omega, USA) with a data acquisition system were responsible for recording inlet, outlet, and wall temperatures every 5s. Fig. 2 shows the geometrical configurations, exploded view of heat sink fabricated via CNC milling, and assembly while Table 1 presents the accuracy of the measuring equipment as well as the heat sink's geometrical dimensions. To compute the pressure difference, a pressure transducer is installed in a parallel way across the heat sink. Finally, the heated water passed through a radiator installed in-between the heat sink and storage tank to release the heat and put back into the storage tank.

3. Data processing

3.1. Hydraulic diameter

For heat sinks with varying cross-sectional area, the most generally employed technique, which is hydraulic diameter equal to four times the area divided by the perimeter, is ineffective. The hydraulic diameter of particularly designed inline and staggered geometrical configurations has been computed using the same technique used by Chen et al. [24]. Cui et al. [19] adopted this approach to compute the hydraulic diameter while numerically analyzing the performance of airfoil shape utilizing supercritical CO_2 as a cooling agent. The specific sections of both configurations need to be considered, as shown in Fig. 3. The hydraulic diameter can be calculated dividing this volume by the wetted area (A_w) or the sum of all surface areas excluding the surface normal to the flow direction. The following set of Eqs. ((1)–(3)) have been used to compute the hydraulic diameter (h_d).

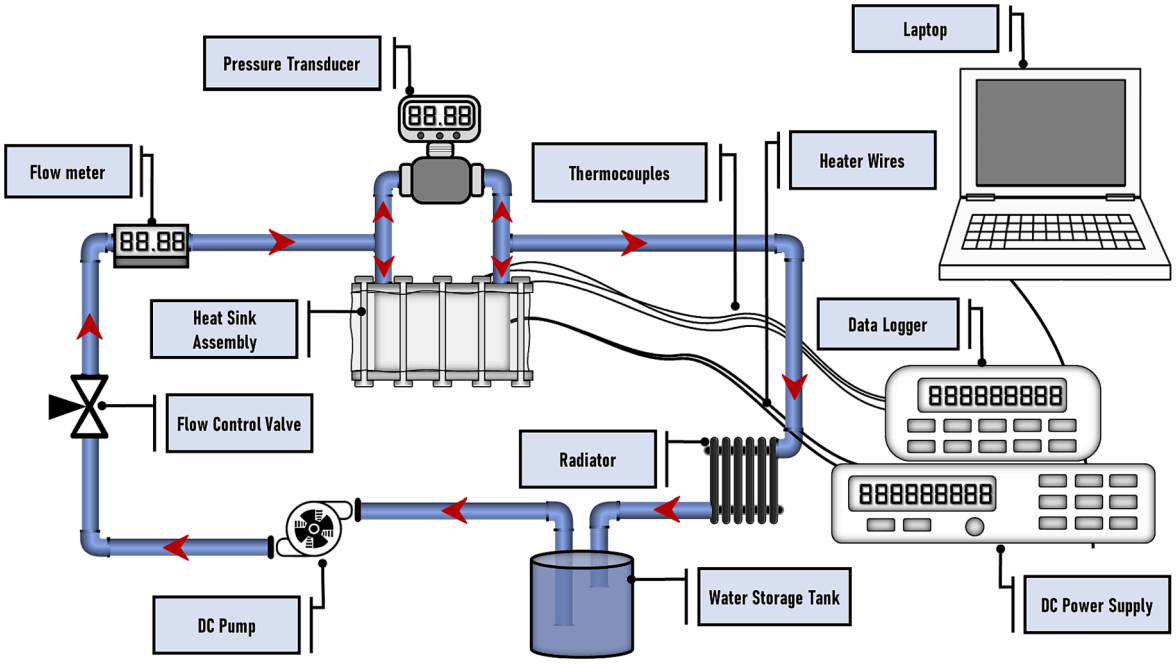

Fig. 1. Schematic illustration of coolant flow cycle and experimental setup.

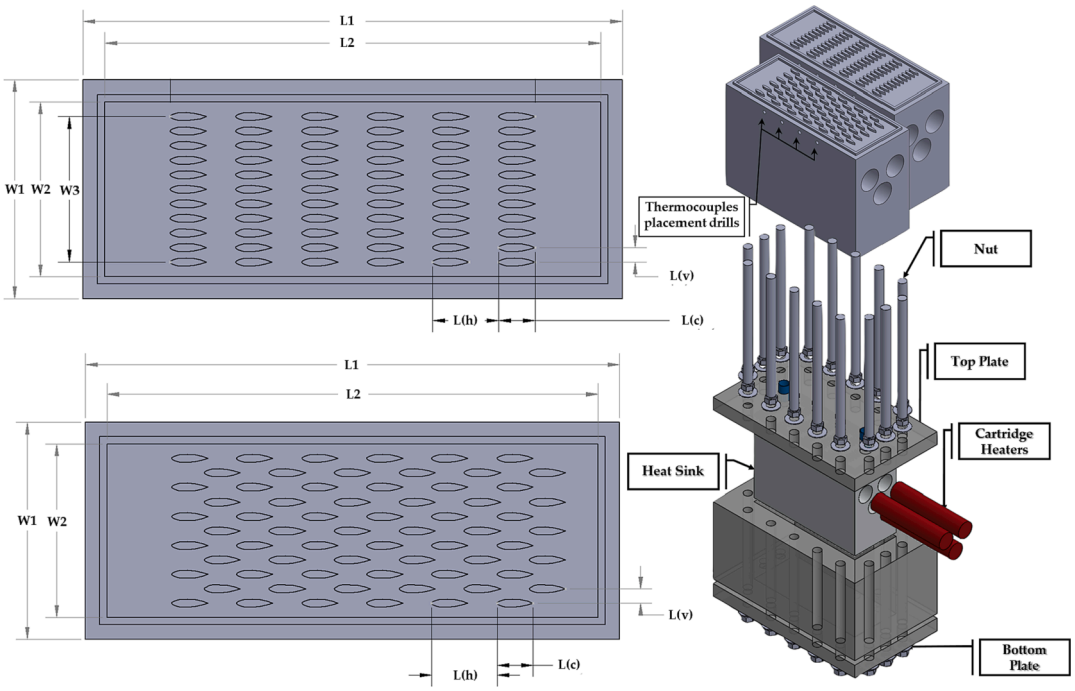

Fig. 2. Heat sinks geometrical configurations, exploded view, and assembly.

Table 1
Measuring equipment and heat sink's geometrical parameters.

Measuring Equipment			Geometrical configuration	
Instrument	Range	Accuracy	Parameter	Dimension (mm)
Thermocouple	0–300 °C	±0.1 °C	L1 × L2	74 × 68
Flow Meter	0.2–2 l/min	±6 %	W1 × W2 × W3	30 × 24 × 20
Power Supply	0–120 V	Voltage ±0.04 %	L(v)	2
	0–18 A	Current ±0.1 %	L(c)	5
Pressure Transducer	0–70 mbar	±0.08 %	L(h)	9

$$U_{ss} = (L \times W - A_{s,top})H \tag{1}$$

$$A_w = 2\left(P_{fin} \times H/2\right) + 2\left(L - L_{fin}\right)H + 2\left(L \times W - A_{s,top}\right) \tag{2}$$

$$d_h = \frac{4U_{ss}}{A_w} \tag{3}$$

where L, H, W, U_{ss} represents the length, height, width, and volume of the specific sections, respectively. $A_{s,top}, P_{fin}$, and L_{fin} indicates top surface areas, perimeter, and length of fins, accordingly.

3.2. Performance parameters

The amount of heat transferred (Q) between the flowing fluid and heat sink was computed using Eq. (4).

$$Q = \dot{m}c_p(T_{out} - T_{in}) \tag{4}$$

where $\dot{m}$ is the coolant flow rate, T_{in} and T_{out} are the temperature at inlet and outlet respectively, and c_p is the specific heat capacity of water.

The fluid thermophysical characteristics were computed using the mean bulk temperature (T_m), which was calculated using Eq. (5).

$$T_m = \frac{T_{in} + T_{out}}{2} \tag{5}$$

The temperature measurements were recorded using thermocouples positioned directly below the channel wall. The temperature of the channel wall (T_w) was determined by Eq. (6).

$$T_w = T_b - \left(\frac{Ql_w}{k_s A_w}\right) \tag{6}$$

where T_b, l_w, k_s, and A_w represented the base temperature, distance between the thermocouple and the channel wall, thermal conductivity, and wall surface area, respectively. Eq. (7) provides the value of wall surface area.

$$A_w = L_s \times W_s \tag{7}$$

where L_s and W_s are the length and width of the part being investigated.

Eq. (8) was used to calculate the values of logarithmic mean temperature different (LMTD), while the convective heat transfer coefficient was calculated by Eq. (9) [28].

$$LMTD = \frac{(T_w - T_{inlet}) - (T_w - T_{outlet})}{\ln\left[\frac{(T_w - T_{inlet})}{(T_w - T_{outlet})}\right]} \tag{8}$$

$$h = \left[\frac{mC_p(T_{out} - T_{in})}{A_e \times (LMTD)}\right] \tag{9}$$

A_e is the effective surface area of heat sink.

Eq. (10) was used to calculate the Reynolds number (Re).

$$Re = \frac{\rho v d_h}{\mu} \tag{10}$$

ρ, v, and μ are the coolant density, viscosity, and velocity, respectively.

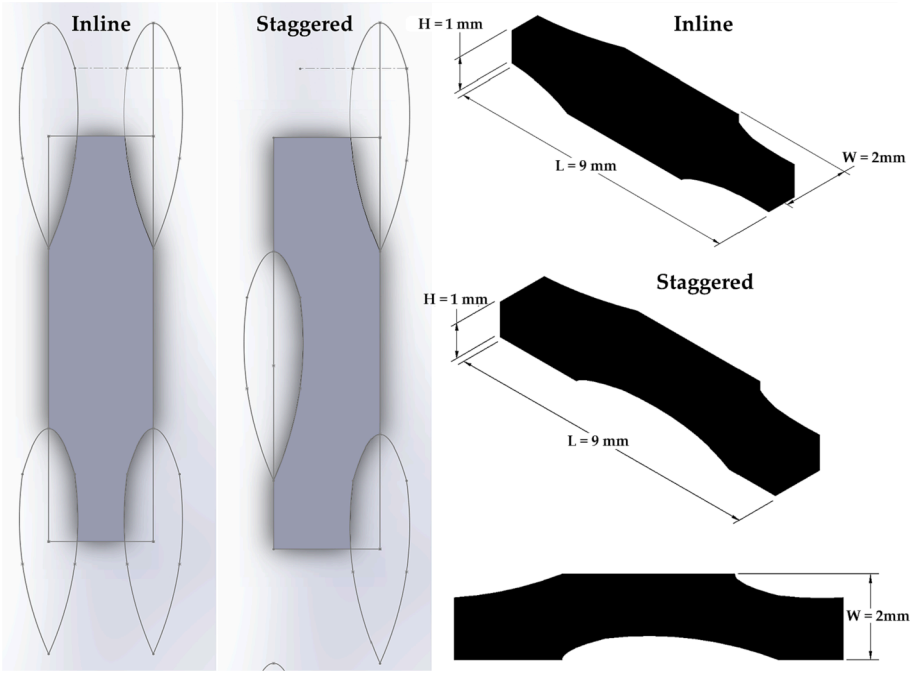

Fig. 3. Inline and staggered configuration specific sections.

However, to compute the average fluid velocity Eq. (11) was applied.

$$v = m/A_{avg.} \tag{11}$$

where $A_{avg.}$ denoted the average cross sectional area, evaluated using the Eq. (12).

$$A_{avg.} = \frac{U_{ss}}{L} \tag{12}$$

Nusselt number (Nu) and thermal resistance (R_{th}) was computed using Eq. (13) and Eq. (14), respectively.

$$Nu = \frac{hd_h}{k_f} \tag{13}$$

$$R_{th} = \frac{LMTD}{Q} \tag{14}$$

where k_f is the working fluid thermal conductivity.

The amount of energy required to pump the fluid through heat sink was calculated by Eq. (15) [29].

$$PumpingPower = PP = V \times \Delta P \tag{15}$$

The volumetric flow rate and pressure drop across the test segment were represented by the symbols V and ΔP respectively.

The overall heat sink performance was computed using the Eq. (16) [30,31].

$$Overallperformance = \frac{Q}{PP} \tag{16}$$

3.3. Uncertainty analysis

For small systems, the uncertainty analysis is recommended to associate the instrumental errors with the experimental measures. The current study estimated the uncertainty in several measuring parameters using the same method as earlier studies [32–34]. The following set of Eqs. ((17)–(21)) give the uncertainty in various parameters. According to the results, Nusselt number, Reynolds Number, and pressure drop maximum values of uncertainty was never observed to be greater than 2.19 %, 5.58 %, and 0.76 %, respectively.

$$\frac{U_h}{h} = \sqrt{\left(\frac{U_Q}{Q}\right)^2 + \left(\frac{U_{(T_w - T_i)}}{(T_w - T_i)}\right)^2 + \left(\frac{U_{(T_w - T_o)}}{(T_w - T_o)}\right)^2 + \left(\frac{U_\rho}{\rho}\right)^2 + \left(\frac{U_{C_p}}{C_p}\right)^2 + \left(\frac{U_{A_b}}{A_b}\right)^2 + \left(\frac{U_v}{v}\right)^2 + \left(\frac{U_{(T_{out} - T_{in})}}{(T_{out} - T_{in})}\right)^2} \tag{17}$$

$$\frac{U_Q}{Q} = \sqrt{\left(\frac{U_V}{V}\right)^2 + \left(\frac{U_I}{I}\right)^2} \tag{18}$$

$$\frac{U_{Nu}}{Nu} = \sqrt{\left(\frac{U_h}{h}\right)^2 + \left(\frac{U_k}{k}\right)^2 + \left(\frac{U_{D_h}}{D_h}\right)^2} \tag{19}$$

$$\frac{U_{Re}}{Re} = \sqrt{\left(\frac{U_\rho}{\rho}\right)^2 + \left(\frac{U_{\overline{V}}}{\overline{V}}\right)^2 + \left(\frac{U_\mu}{\mu}\right)^2} \tag{20}$$

$$\varepsilon_{\Delta P} = \sqrt{\left(\frac{U_{\Delta P}}{\Delta P}\right)^2} \tag{21}$$

4. Results and discussion

The electronic industry is facing challenges to maintain the

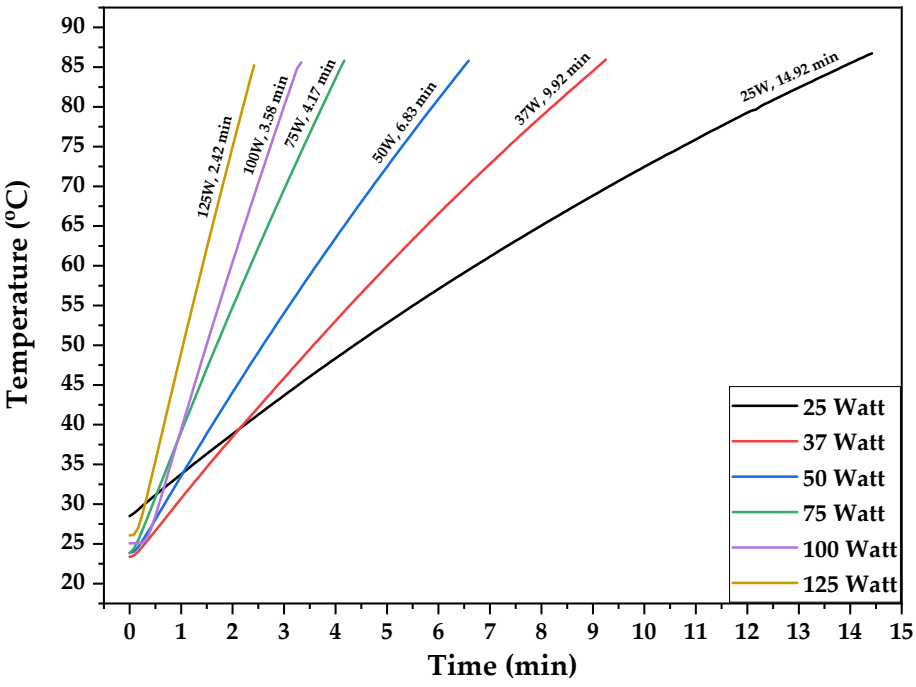

Fig. 4. Temperature variation of heat sink against various heating powers under natural convection conditions.

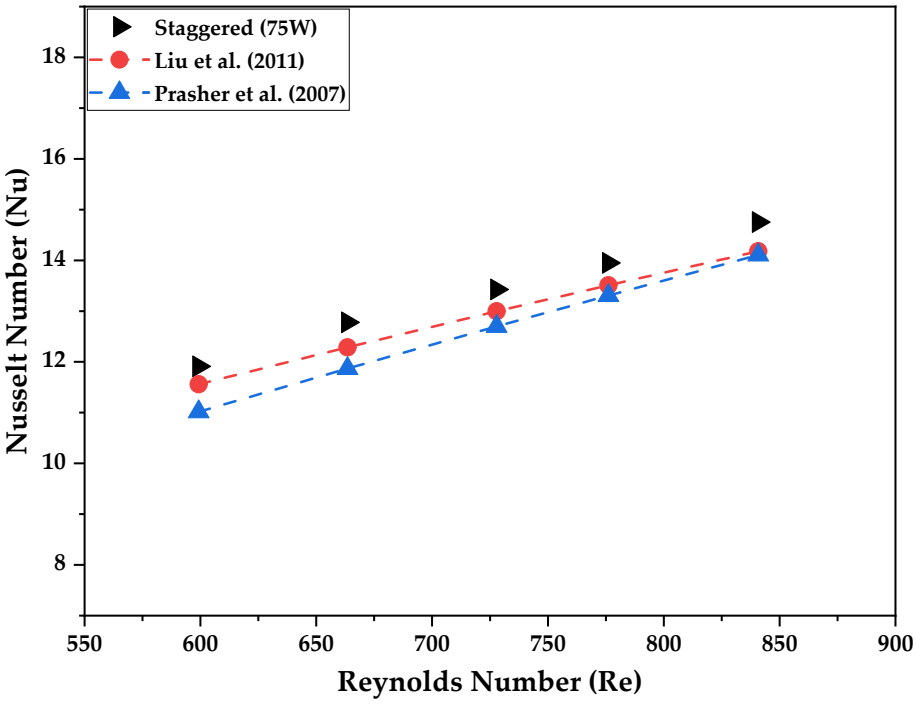

Fig. 5. Nusselt number comparison between experimental and the values predicted with Liu et al. [36] and Prasher et al. [37] correlations.

temperature of devices under 85 °C at 300 W/cm^2 [35]. Convectional techniques failed to provide the desired cooling effect for high heat generating electronic devices and the thermal management of advanced, compact, or integrated devices. A study was carried out to investigate the temperature variation of heat sink at different heating powers under natural convection. Fig. 4 depicts the trend and time took to cross 85 °C in all cases.

The slope of the temperature curve grows as the heating power increases from 25 W to 125 W. At higher heating powers, the particular limit was breached in just 2.42 min, whereas it took about 15 min even at modest heating input. Therefore, natural cooling is found to be ineffective even at low heat flux (~15 kW/m^2). It was concluded that without an efficient and effective cooling system, the temperature of the running equipment exceeded the safe limit quickly.

4.1. Validation

The validation of the experimental rig was conducted by comparing the results with the models developed by Liu et al. [36] and Prasher et al. [37]. It was found that the values predicted using the correlations were

very close to the experimental results, as shown in Fig. 5. Liu et al. [36] conducted a number of experiments on liquid-cooled heat sink considering various parameters and proposed a general correlation to predict the Nusselt number against flow rate, represented by Eq. (22). Prasher et al. [37] studied the staggered arrangement of fins varying Re in the range of 40–1000. They ran a series of tests and derived a correlation model for average Nusselt number, which is given by Eq (23). The correlations used have taken into account the geometric configuration of the heat sink for the prediction of Nusselt number values and reported in various studies to validate the results [12,38,39]. The friction factor (f) was computed from the pressure drop values using Eq. (24) [40,41]. To validate the experimental pressure drop values, the calculated friction factor was compared with the values estimated using the model of Gunther and Shaw [42], presented with Eq. (25). The derived model of Gunther and Shaw [42] has been reported in various studies to predict the values of friction factor using pressure drop and vice versa [43–45]. However, to estimate the deviation, mean relative error (MRE) was computed using Eq. (26) [46]. According to the results, the model of Liu et al. [36] predicted the experimental values with a MRE of 3.41 %, while the model of Prasher et al. [37] projected the results with an error of 6.19 %. In addition, the model of Gunther and Shaw [42] predicted all the values of friction factors with a MRE of 7.6 %, as shown in Fig. 6.

$$Nu = 0.281Re^{0.73}\left(\frac{S_L - d_f}{d_f}\right)^{-0.63} \tag{22}$$

$$Nu = 0.1245Re^{0.6106}\left(\frac{Pr}{Pr_s}\right)^{0.25} Pr^{0.36} \tag{23}$$

$$f = \frac{\Delta P}{n\rho.\frac{v^2}{2}} \tag{24}$$

$$f = \frac{180}{Re}\left(\frac{4t_p l_p}{\pi d_f} - 1\right)^{0.4}\left(\frac{l_p}{t_p}\right)^{0.6} \tag{25}$$

$$\text{Mean Relative Error (MRE)} = \frac{1}{N}\sum_{j=1}^{N}\left[\frac{\left|U_{exp.} - U_{pred.}\right|}{U_{exp.}}\right] \times 100\% \tag{26}$$

where $n, l_p, d_f, t_p, Pr_s, N, U_{exp.}$, and $U_{pred.}$ are the fins number of rows, longitudinal pitch, fin hydraulic diameter, transverse pitch, surface Prandtl number, total number of data points, experimental values, and predicted values, respectively. The inline and staggered arrangements are shown in Fig. 7 to clarify the longitudinal and transverse pitch.

4.2. Nusselt number

Fig. 8 depicts the variation of Nusselt number with Reynolds number at three different heating powers of 75, 100, and 125 W. The thermal performance of inline geometry was found to be better at all flow rates evaluated, however, this increase was irregular. According to the results, the maximum improvement of 4.82 % was observed in Nusselt number for inline configuration compared to the staggered arrangement. This could be due to the fact that the staggered arrangement can make the flow more smother and preclude the development of vortex separation. In addition, inline arrangement provides a narrower passage for fluid flow which could cause an increase in heat transfer with a considerable penalty of pumping power. Fig. 9 shows the passage of fluid for the case of inline and staggered arrangements. The numerical study conducted by Xu et al. [25] was also observed the same effect while investigating the inline and staggered arrangement of airfoil shaped pin fins employing supercritical CO_2 as a working fluid. The highest value of Nusselt number was found to be 15.86 and 15.23 for inline and staggered arrangement respectively at maximum flow rate and heating power.

4.3. Wall temperature

As the Nusselt number of inline heat sink is comparatively higher, a slight reduction in wall temperature was also noticed. The wall temperatures of both arrangements are shown in Fig. 10(a) as a function of Reynolds number. At each of the heating powers, the wall temperature was never found to be higher than 50 °C, the maximum was observed at lowest flow rate and decreased as flow rates increased. The maximum value of 41.63 °C was noticed at lowest flow rate and maximum heating power. In addition, the minimal wall temperature values are plotted in

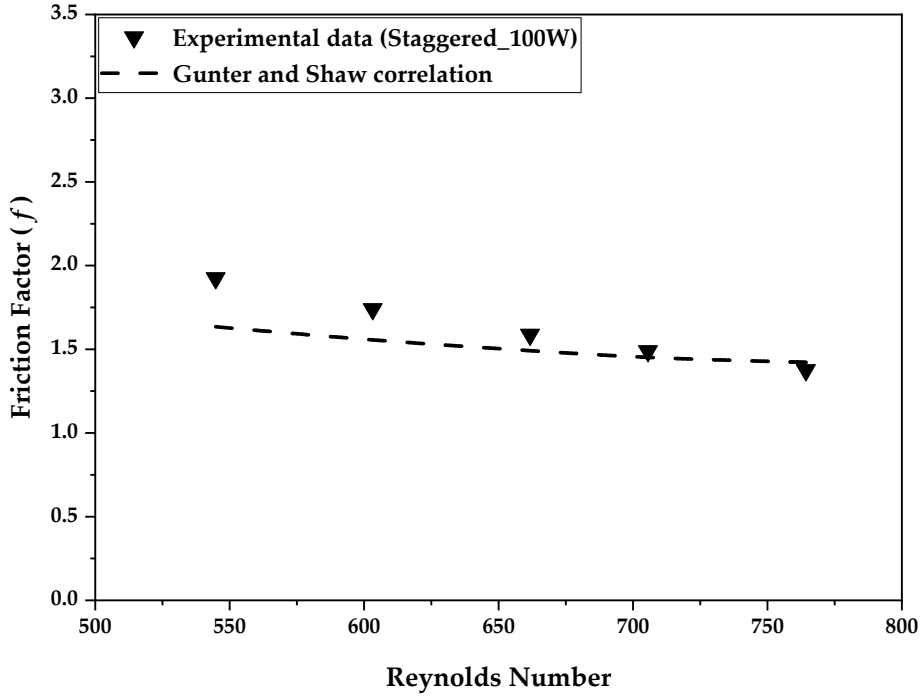

Fig. 6. Comparison of friction factor with the values predicted using Gunter and Shaw [42] model.

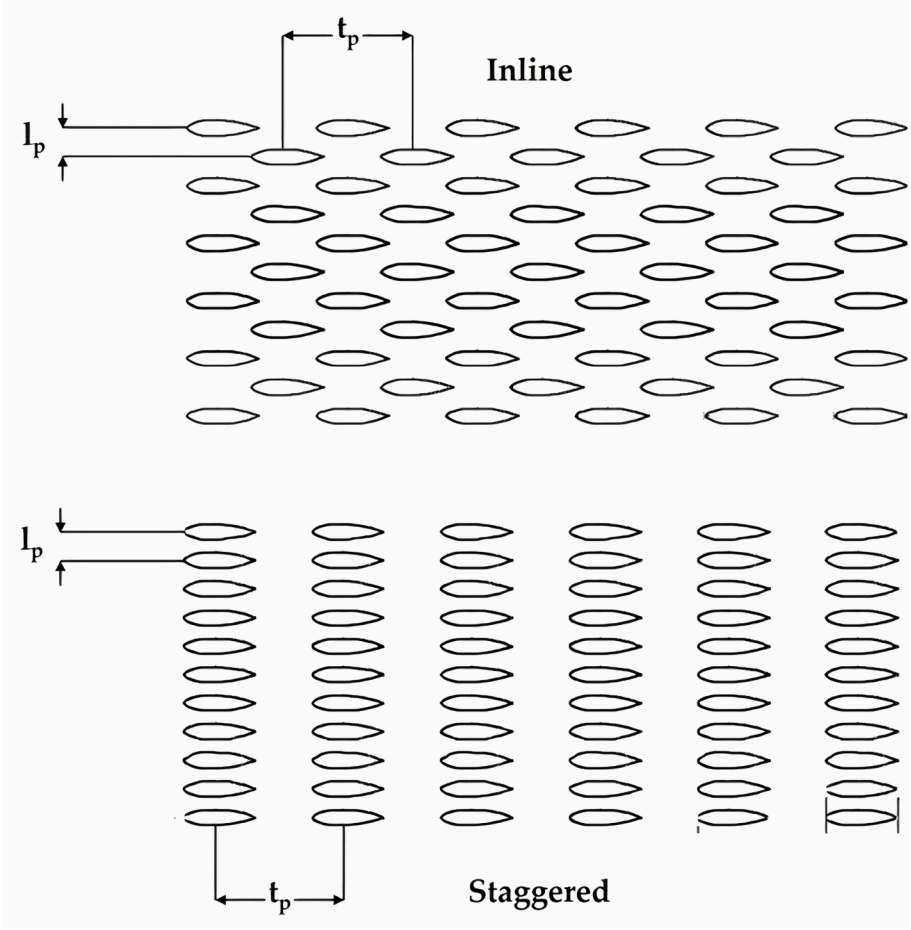

Fig. 7. Longitudinal and transverse pitch clarification.

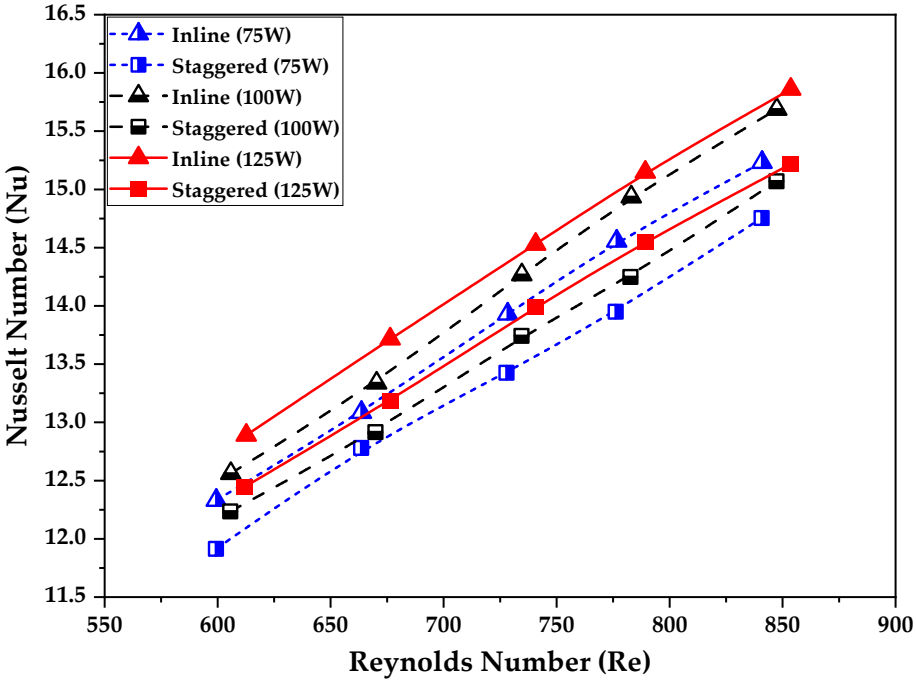

Fig. 8. Nusselt number variation for different geometric configurations of heat sinks against Reynolds number.

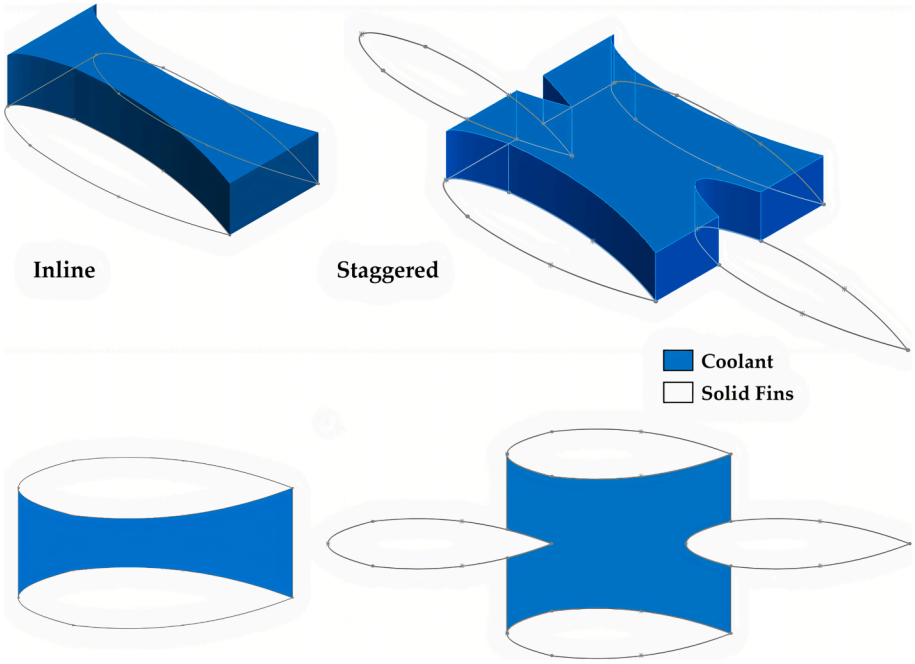

Fig. 9. Fluid flow passage of inline and staggered geometrical configurations.

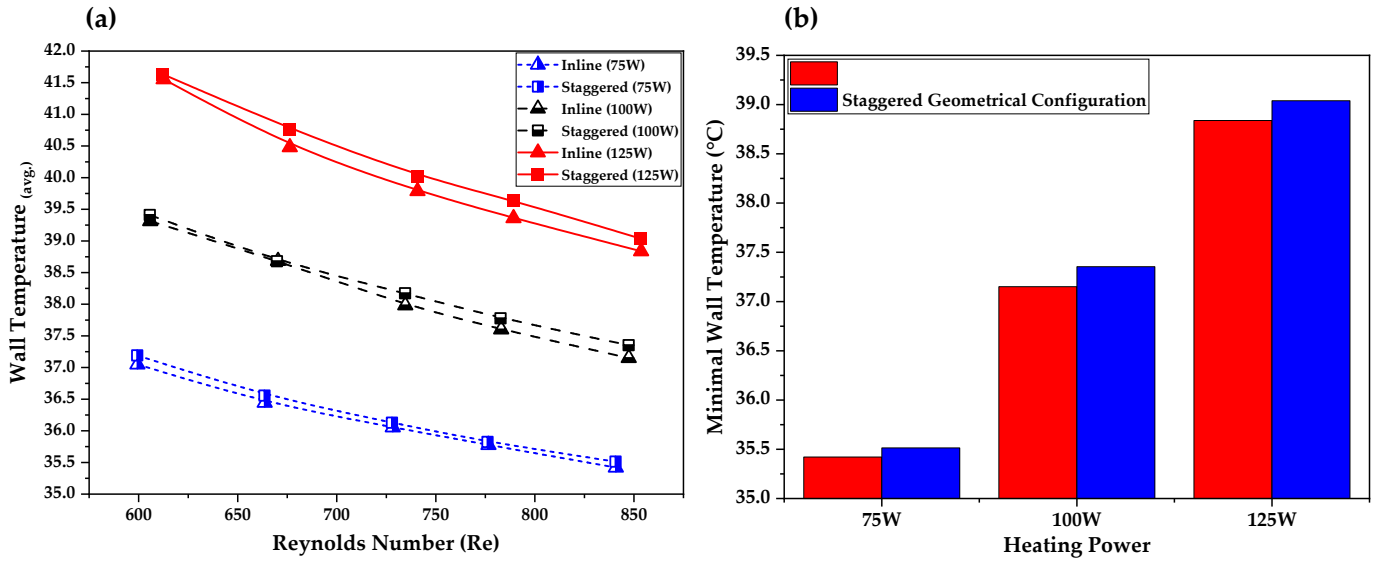

Fig. 10. (a) Variation of wall temperature with Reynolds number at various heating powers, (b) Minimal wall temperature against different heating powers.

Fig. 10(b) at each power, which exhibits a significant increase in sink wall temperature with the increase in supplied heat. The minimum wall temperature was observed to be around 35.42 °C and 35.51 °C at 75 W for inline and staggered configurations, respectively. In comparison, the difference in wall temperature was very small, the maximum it was about 0.71 %.

4.4. Thermal resistance and log mean temperature difference (LMTD)

One of the most important criteria to consider when evaluating the performance of a heat sink is thermal resistance. It is inversely proportional to the rate of heat transfer and is directly related to the LMTD. As illustrated in Fig. 11, the thermal resistance of an inline arrangement of pin fins was marginally lower than that of a staggered arrangement due to the higher rate of heat transfer and a lower value of LMTD. For both configurations, the maximum value of thermal resistance and LMTD was observed at the lowest Reynolds number, and it was found to be reduced as the Reynolds number increased. Overall, with the increase in heating power LMTD was observed to be increased while thermal resistance reduced.

The least values of these parameters at various heating powers are shown in Fig. 12. It was concluded that at each heating power the maximum values were obtained at the lowest Reynolds number. The value of thermal resistance for inline configuration was almost 3.45 %, 3.74 %, and 3.97 % lesser in average than staggered sink at 75 W, 100 W, and 125 W, respectively. Furthermore, for LMTD it was about 2.33 %, 2.60 %, and 3.21 % lower for the inline design.

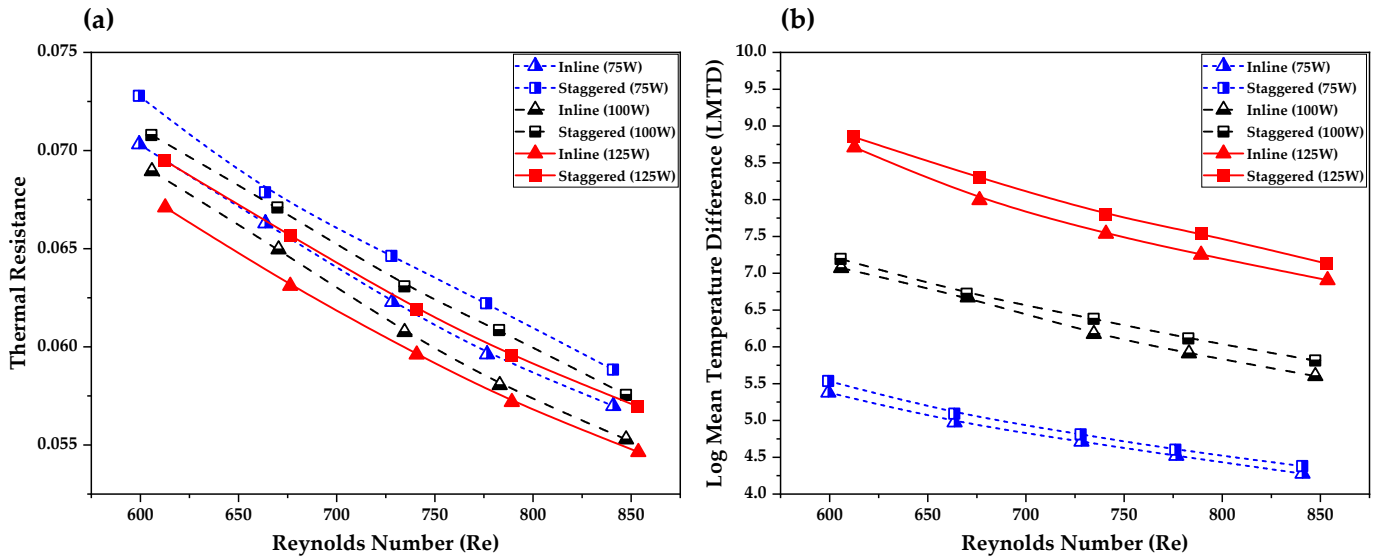

Fig. 11. Variation of thermal resistance for different geometric configurations of heat sinks against Reynolds number.

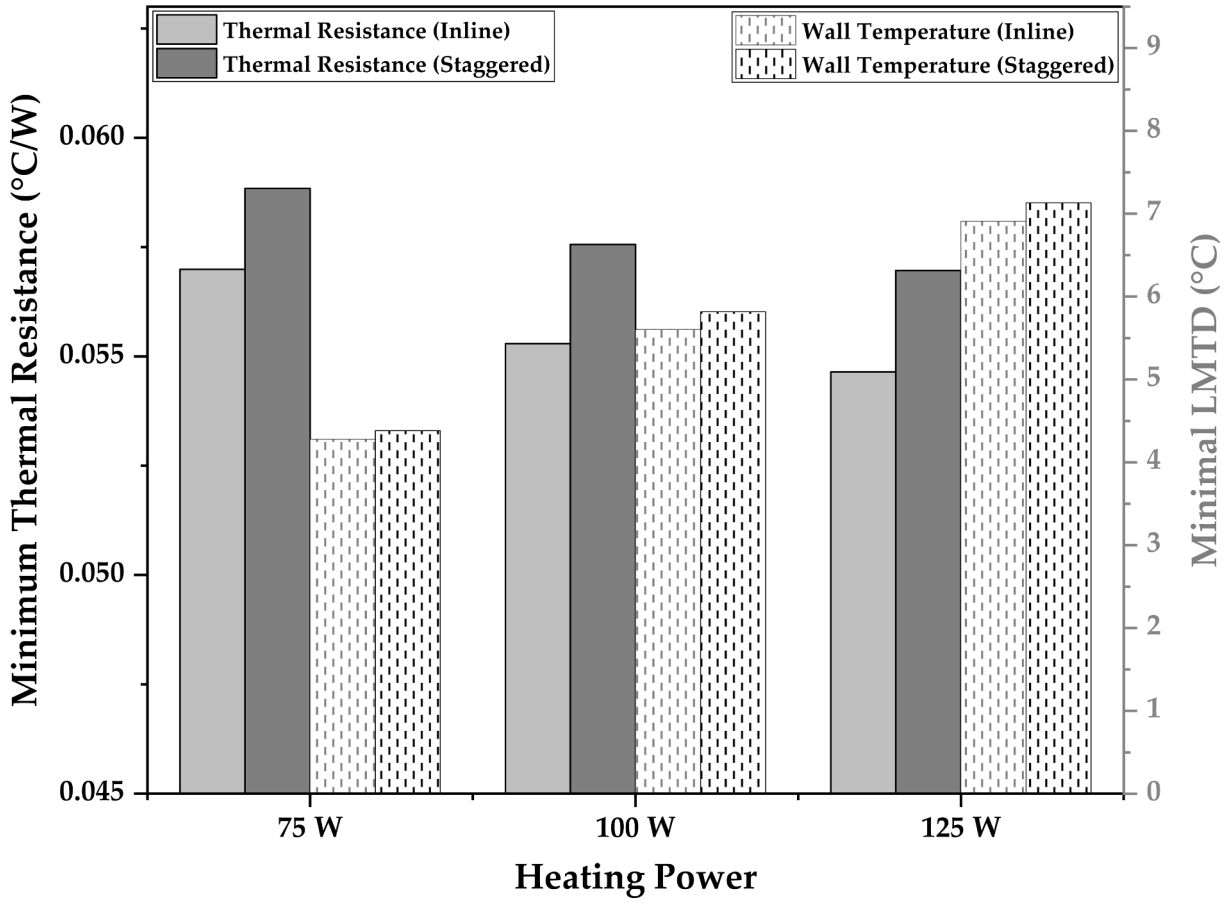

Fig. 12. Minimal values of thermal resistance and LMTD at various heating powers.

4.5. *Pumping power*

In comparison of staggered configuration, the increase in pumping power for inline configuration was noticeably higher than staggered configuration. Most of the studies conducted on different shapes of pin fins observed more flow resistance in staggered arrangement of pin fins. However, in the particular case of airfoil shaped pin fins, due to the wider leading edge and narrower trailing edge staggered arrangement offered less resistance to flow than that of inline arrangement [25]. Furthermore, as shown in Fig. 9, the fluid passage is narrower for inline configuration, whereas it is comparatively wider for the case of staggered arrangement. Consequently, staggered arrangement showed a comparatively lower pressure drop. It was noted that pressure drop increased with the increase of Reynolds number which results an

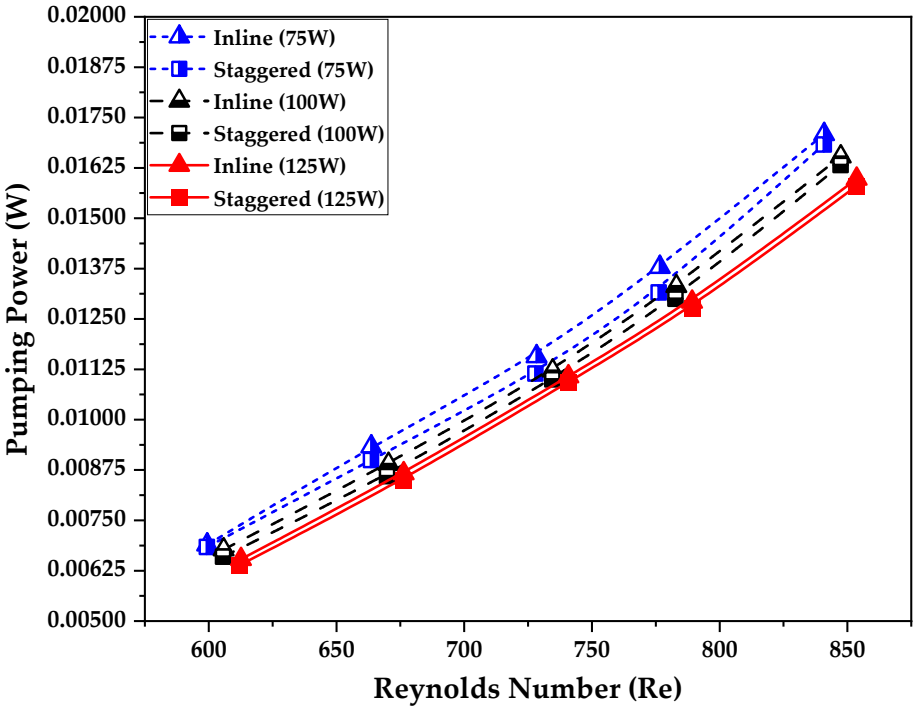

Fig. 13. Pumping power variation with Reynolds Number.

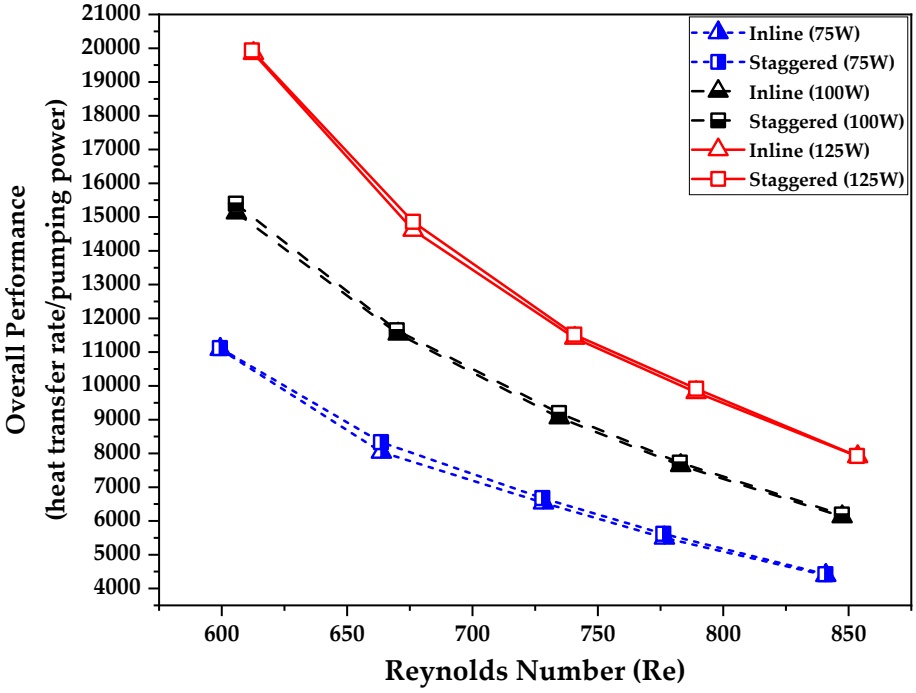

Fig. 14. Overall performance variation for different geometric configurations of heat sinks against Reynolds number.

increase in pumping power, as shown in Fig. 13.

A noticeable decreased in pumping power was also observed with the increase in heating power, this could be due to the decrease in fluid density. The maximum value of pumping power for inline and staggered arrangement was around 0.0171 W and 0.0169 W, respectively at minimum heating power, while the least value was about 0.01598 W and 0.0158 W at maximum applied heating power.

4.6. *Overall performance*

It should be noted that we may not infer which arrangement of pin fins provides superior results just on the basis of heat transfer while it is the trade-off pumping power and heat transfer enhancement. To draw the comprehensive comparison of sinks, the overall performance was evaluated that considered both pumping power and heat transfer simultaneously. This factor took into account both parameters as it is the ratio of heat transfer rate to pumping power.

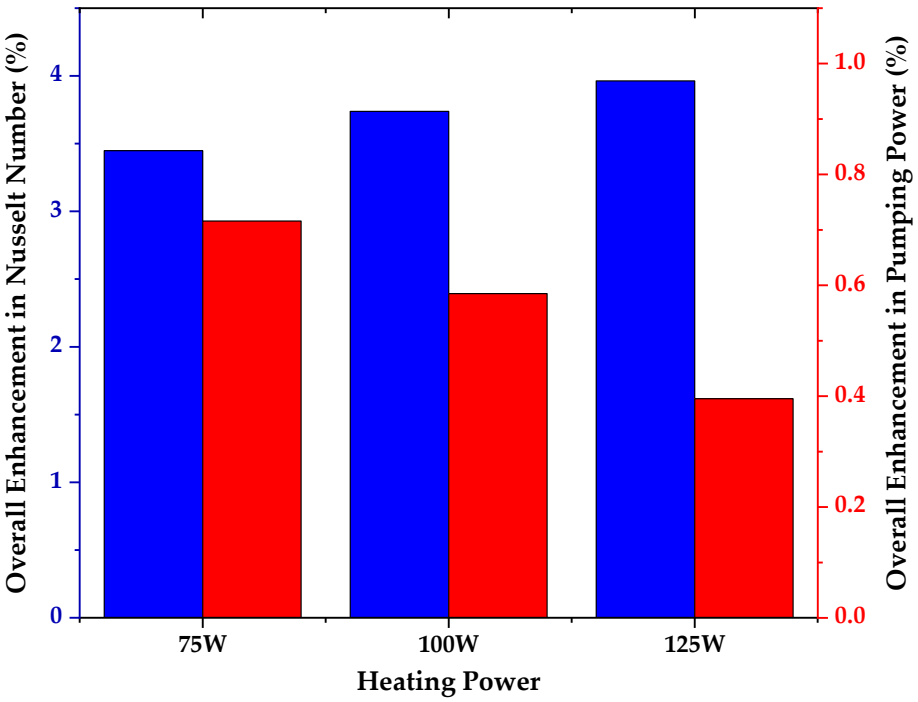

Fig. 15. Overall enhancement in Nusselt number and pumping power at various heating powers.

The staggered geometrical configuration offers wider space to fluid flow resulting in a comparatively little pressure decrease from inlet to outlet. Results revealed that the overall performance of staggered geometry was slightly better than line arrangement, as shown in Fig. 14.

A noticeable decrease in overall performance was observed with the increase in flow rate. Furthermore, increasing heating power can improve the overall performance at all flowrates. The maximum values of overall performance were found at the lowest Reynolds number and higher heating power. In comparison, the average enhancement of 1.81 %, 1.25 %, and 0.87 % in overall performance was observed for staggered arrangement at 75 W, 100 W, 125 W, respectively. Instead of that inline arrangement of airfoil shaped pin-fins showed better thermal characteristics, it is recommended to use the staggered arrangement based on better overall performance.

4.7. Heating power

The comparative study revealed that the heating power has a significant impact on Nusselt number improvement and pumping power reduction, as shown in Fig. 15. The overall improvement in Nusselt number for inline arrangement was found to enhance with input power, however the overall pumping power was observed to reduce as the pressure drop decreased with increasing input heat. The maximum overall increase in the Nusselt number of inline geometry was determined to be approximately 3.96 % at 125 W, whereas the utmost penalty in pumping power was around 2.93 % at 75 W. Results also yielded that the reduction in pumping power from 100 W to 125 W was considerably greater than the drop observed when power was changed from 75 W to 100 W. However, for the case of Nusselt number, the improvement from 75 W to 100 W was greater than the rise from 100 W to 125 W.

5. Concluding remarks

The hydrothermal performance of heat sink is explored experimentally by altering the position of airfoil shaped pin fins. A noticeable impact of geometrical configuration on thermal and hydraulic performance of heat sink was observed. In comparison to inline arrangement, the heat sink with staggered arrangement of pin fins was found to be more lucrative. The experimental findings can be summarized as follows:

- Inline geometrical configuration showed better thermal characteristics. Inline geometry has always been observed to have a higher rate of heat transfer. Furthermore, thermal resistance and wall temperature was found to be slightly less for inline configurations.
- It is recommended to consider the inline configuration if heat transfer is the major concern and the penalty of pumping power is bearable. The maximum overall wall temperature of about 40.01 °C and 40.22 °C was observed at 125 W for inline and staggered configurations, respectively. Thermal resistance was maximum at the lowest heating power 75 W, averaging around 0.0631 °C/W and 0.0653 °C/W for inline and staggered arrangements.
- For both geometrical configurations, a significant increase in Nusselt number was observed with Reynolds number and heating power. However, the improvement in heat transfer from 75 W to 100 W was comparatively more than the increase from 100 W to 125 W. For inline geometry, the highest Nu value was approximately 15.86 at 125 W, whereas it was around 15.21 for staggered arrangement. In comparison of staggered geometry, the overall improvement in Nusselt number for inline heat sinks was about 3.96 %.
- Pressure drop in inline geometry was found to be higher as the layout of inline geometry offers narrower passage for fluid flow, which incurs a penalty in the form of pumping power. In addition, pumping power augmented as the Reynolds number increased, but decreased with increasing heating power. The overall pumping power of inline design was found to be 2.93 % higher than that of staggered design.
- The overall performance of staggered arrangement was attained to be more at all heating powers and flow rates. It was found to increase as heating power increased while decreasing substantially with Reynolds number. The staggered heat sink outperformed the inline heat sink by 1.81 % at the lowest studied heating power.
- Staggered arrangement improves thermal management offering smoother fluid flow. In parallel arrangement due to continual contraction and expansion, nonuniformity in flow and temperature is more prominent.

The finding of this experimental study will be very helpful in the development of heat sinks that offer less fluid resistance while exhibiting remarkable thermal performance. It is recommended to further investigate this shape by changing the positioning, transverse and longitudinal pitch, fins angle, etc. In future, such kind of shapes can be studied in conjunction with other pin-fins (for example, a heat sink having multiple pin-fin shapes), inside straight channels, with grooves, etc.

CRediT authorship contribution statement

Hamza Babar: Methodology, Data curation, Formal analysis, Investigation, Validation, Writing - original draft. **Hongwei Wu:** Conceptualization, Supervision. **Hafiz Muhammad Ali:** Conceptualization, Supervision.

Declaration of Competing Interest

The authors declare that they have no known competing financial interests or personal relationships that could have appeared to influence the work reported in this paper.

Data availability

Data will be made available on request.

References

[1] C.S. Sharma, M.K. Tiwari, S. Zimmermann, T. Brunschwiler, G. Schlottig, B. Michel, D. Poulikakos, Energy efficient hotspot-targeted embedded liquid cooling of electronics, Appl. Energy 138 (2015) 414–422, https://doi.org/10.1016/j.apenergy.2014.10.068.

[2] C. Batunlu, A. Albarbar, Real-time system for monitoring the electro-thermal behaviour of power electronic devices used in boost converters, Microelectron. Reliab. 62 (2016) 82–90, https://doi.org/10.1016/j.microrel.2016.03.033.

[3] Y. Deng, M. Zhang, Y. Jiang, J. Liu, Two-stage multichannel liquid–metal cooling system for thermal management of high-heat-flux-density chip array, Energy Convers Manage. 259 (2022), 115591, https://doi.org/10.1016/j.enconman.2022.115591.

[4] J. Gao, Z. Hu, Q. Yang, X. Liang, H. Wu, Fluid flow and heat transfer in microchannel heat sinks: modelling review and recent progress, Therm. Sci. Eng. Prog. 29 (2022), 101203, https://doi.org/10.1016/j.tsep.2022.101203.

[5] H.E. Ahmed, B.H. Salman, A.S. Kherbeet, M.I. Ahmed, Optimization of thermal design of heat sinks: a review, Int. J. Heat Mass Transf. 118 (2018) 129–153, https://doi.org/10.1016/j.ijheatmasstransfer.2017.10.099.

[6] G. Sriharan, S. Harikrishnan, H.F. Oztop, Performance improvement of the mini hexagonal tube heat sink using nanofluids, Therm. Sci. Eng. Prog. 34 (2022), 101390, https://doi.org/10.1016/j.tsep.2022.101390.

[7] G. Xie, Y. Li, F. Zhang, B. Sundén, Analysis of micro-channel heat sinks with rectangular-shaped flow obstructions, Numer. Heat Transf. A: Appl. 69 (2016) 335–351, https://doi.org/10.1080/10407782.2015.1080580.

[8] L. Chai, G.D. Xia, H.S. Wang, Laminar flow and heat transfer characteristics of interrupted microchannel heat sink with ribs in the transverse microchambers, Int. J. Therm. Sci. 110 (2016) 1–11, https://doi.org/10.1016/j.ijthermalsci.2016.06.029.

[9] S. Wu, K. Zhang, G. Song, J. Zhu, B. Yao, Experimental study on the performance of a tree-shaped mini-channel liquid cooling heat sink, Case Stud. Therm. Eng. 30 (2022), 101780, https://doi.org/10.1016/j.csite.2022.101780.

[10] F.J. Hong, P. Cheng, H. Ge, G.T. Joo, Conjugate heat transfer in fractal-shaped microchannel network heat sink for integrated microelectronic cooling application, Int. J. Heat Mass Transf. 50 (2007) 4986–4998, https://doi.org/10.1016/j.ijheatmasstransfer.2007.09.006.

[11] T.C. Hung, Y.X. Huang, W.M. Yan, Thermal performance analysis of porous-microchannel heat sinks with different configuration designs, Int. J. Heat Mass Transf. 66 (2013) 235–243, https://doi.org/10.1016/j.ijheatmasstransfer.2013.07.019.

[12] J.F. Tullius, T.K. Tullius, Y. Bayazitoglu, Optimization of short micro pin fins in minichannels, Int. J. Heat Mass Transf. 55 (2012) 3921–3932, https://doi.org/10.1016/j.ijheatmasstransfer.2012.03.022.

[13] S.A. Jajja, W. Ali, H.M. Ali, A.M. Ali, Water cooled minichannel heat sinks for microprocessor cooling: effect of fin spacing, Appl. Therm. Eng. 64 (2014) 76–82, https://doi.org/10.1016/j.applthermaleng.2013.12.007.

[14] A.P. Sudheer, U. Madanan, Numerical investigation into heat transfer augmentation in a square minichannel heat sink using butterfly inserts, Therm. Sci. Eng. Prog. 36 (2022), 101522, https://doi.org/10.1016/j.tsep.2022.101522.

[15] Z. Tang, C. Qi, Z. Tian, L. Chen, Thermal management of electronic components based on new wave bio-inspired structures and nanofluids, Int. Commun. Heat Mass Transf. 131 (2022), 105840, https://doi.org/10.1016/j.icheatmasstransfer.2021.105840.

[16] H.M. Ali, W. Arshad, Thermal performance investigation of staggered and inline pin fin heat sinks using water based rutile and anatase TiO_2 nanofluids, Energy Convers. Manage. 106 (2015) 793–803, https://doi.org/10.1016/j.enconman.2015.10.015.

[17] Y. Yan, T. Zhao, Z. He, Z. Yang, L. Zhang, Numerical investigation on the characteristics of flow and heat transfer enhancement by micro pin-fin array heat sink with fin-shaped strips, Chem. Eng. Process Process Intesif. 160 (2021), 108273, https://doi.org/10.1016/j.cep.2020.108273.

[18] A. Maji, D. Bhanja, P.K. Patowari, Numerical investigation on heat transfer enhancement of heat sink using perforated pin fins with inline and staggered arrangement, Appl. Therm. Eng. 125 (2017) 596–616, https://doi.org/10.1016/j.applthermaleng.2017.07.053.

[19] X. Cui, J. Guo, X. Huai, K. Cheng, H. Zhang, M. Xiang, Numerical study on novel airfoil fins for printed circuit heat exchanger using supercritical CO_2, Int. J. Heat Mass Transf. 121 (2018) 354–366, https://doi.org/10.1016/j.ijheatmasstransfer.2018.01.015.

[20] Y. Li, K. Tagawa, F. Feng, Q. Li, Q. He, A wind tunnel experimental study of icing on wind turbine blade airfoil, Energy Convers. Manage. 85 (2014) 591–595, https://doi.org/10.1016/j.enconman.2014.05.026.

[21] A. Abdelwahab, An airfoil diffuser with variable stagger and solidity for centrifugal compressor applications, Proc. ASME Turbo Expo. 6 (2007) 1117–1127, https://doi.org/10.1115/GT2007-27920.

[22] A. Buljac, I. Džijan, I. Korade, S. Krizmanić, H. Kozmar, Automobile aerodynamics influenced by airfoil-shaped rear wing, Int. J. Automot. Technol. 17 (2016) 377–385, https://doi.org/10.1007/s12239-016-0039-4.

[23] N. Cheriet, H. Amirat, A. Korichi, G. Polidori, Conjugate heat transfer enhancement over heated blocks using airfoil deflectors, Therm. Sci. Eng. Prog. 25 (2021), 101011, https://doi.org/10.1016/j.tsep.2021.101011.

[24] F. Chen, L. Zhang, X. Huai, J. Li, H. Zhang, Z. Liu, Comprehensive performance comparison of airfoil fin PCHEs with NACA 00XX series airfoil, Nucl. Eng. Des. 315 (2017) 42–50, https://doi.org/10.1016/j.nucengdes.2017.02.014.

[25] X. Xu, T. Ma, L. Li, M. Zeng, Y. Chen, Y. Huang, Q. Wang, Optimization of fin arrangement and channel configuration in an airfoil fin PCHE for supercritical CO_2 cycle, Appl. Therm. Eng. 70 (2014) 867–875, https://doi.org/10.1016/j.applthermaleng.2014.05.040.

[26] A. Koşar, Y. Peles, Convective flow of refrigerant (R-123) across a bank of micro pin fins, Int. J. Heat Mass Transf. 49 (2006) 3142–3155, https://doi.org/10.1016/j.ijheatmasstransfer.2006.02.013.

[27] J.Y. Ho, K.K. Wong, K.C. Leong, T.N. Wong, Convective heat transfer performance of airfoil heat sinks fabricated by selective laser melting, Int. J. Therm. Sci. 114 (2017) 213–228, https://doi.org/10.1016/j.ijthermalsci.2016.12.016.

[28] Z. Chamanroy, M. Khoshvaght-Aliabadi, Analysis of straight and wavy miniature heat sinks equipped with straight and wavy pin-fins, Int. J. Therm. Sci. 146 (2019), 106071, https://doi.org/10.1016/j.ijthermalsci.2019.106071.

[29] M. Bahiraei, S. Heshmatian, Application of a novel biological nanofluid in a liquid block heat sink for cooling of an electronic processor: thermal performance and irreversibility considerations, Energy Convers. Manage. 149 (2017) 155–167, https://doi.org/10.1016/j.enconman.2017.07.020.

[30] M. Khoshvaght-Aliabadi, M. Sahamiyan, M. Hesampour, O. Sartipzadeh, Experimental study on cooling performance of sinusoidal–wavy minichannel heat sink, Appl. Therm. Eng. 92 (2016) 50–61, https://doi.org/10.1016/j.applthermaleng.2015.09.015.

[31] M.U. Sajid, H.M. Ali, A. Sufyan, D. Rashid, S.U. Zahid, W.U. Rehman, Experimental investigation of TiO_2–water nanofluid flow and heat transfer inside wavy mini-channel heat sinks, J. Therm. Anal. Calorim. 137 (2019) 1279–1294, https://doi.org/10.1007/s10973-019-08043-9.

[32] I.A. Zakaria, W.A.N.W. Mohamed, M.B. Zailan, W.H. Azmi, Experimental analysis of SiO_2-distilled water nanofluids in a polymer electrolyte membrane fuel cell parallel channel cooling plate, Int. J. Hydrogen Energy 44 (2019) 25850–25862, https://doi.org/10.1016/j.ijhydene.2019.07.255.

[33] H.W. Coleman, W.G. Steele, Experimentation, Validation, and Uncertainty Analysis for Engineers, John Wiley & Sons, 2018.

[34] W.H. Azmi, K.V. Sharma, P.K. Sarma, R. Mamat, G. Najafi, Heat transfer and friction factor of water based TiO_2 and SiO_2 nanofluids under turbulent flow in a tube, Int. Commun. Heat Mass Transf. 59 (2014) 30–38.

[35] B. Agostini, M. Fabbri, J.E. Park, L. Wojtan, J.R. Thome, B. Michel, State of the art of high heat flux cooling technologies, Heat Transf. Eng. 28 (2007) 258–281, https://doi.org/10.1080/01457630601117799.

[36] M. Liu, D. Liu, S. Xu, Y. Chen, Experimental study on liquid flow and heat transfer in micro square pin fin heat sink, Int. J. Heat Mass Transf. 54 (2011) 5602–5611, https://doi.org/10.1016/j.ijheatmasstransfer.2011.07.013.

[37] R.S. Prasher, J. Dirner, J.-Y. Chang, A. Myers, D. Chau, D. He, S. Prstic, Nusselt number and friction factor of staggered arrays of low aspect ratio micropin-fins under cross flow for water as fluid, J. Heat Transf. 129 (2007) 141–153, https://doi.org/10.1115/1.2402179.

[38] J. Zhang, Y. Zhao, Y. Diao, Y. Zhang, An experimental study on fluid flow and heat transfer in a multiport minichannel flat tube with micro-fin structures, Int. J. Heat Mass Transf. 84 (2015) 511–520, https://doi.org/10.1016/j.ijheatmasstransfer.2015.01.049.

[39] S. Nawaz, H. Babar, H.M. Ali, M.U. Sajid, M.M. Janjua, Z. Said, A.K. Tiwari, L. Syam Sundar, C. Li, Oriented square shaped pin-fin heat sink: performance evaluation employing mixture based on ethylene glycol/water graphene oxide nanofluid, Appl. Therm. Eng. 206 (2022), 118085, https://doi.org/10.1016/j.applthermaleng.2022.118085.

[40] E. Rasouli, C. Naderi, V. Narayanan, Pitch and aspect ratio effects on single-phase heat transfer through microscale pin fin heat sinks, Int. J. Heat Mass Transf. 118 (2018) 416–428, https://doi.org/10.1016/j.ijheatmasstransfer.2017.10.105.
[41] A. Kosar, C.-J. Kuo, Y. Peles, Hydoroil-based micro pin fin heat sink, in: Proceedings of IMECE, 2008, pp. 563–570, https://doi.org/10.1115/imece2006-13257.
[42] A.Y. Gunter, W.A. Shaw, A general correlation of friction factors for various types of surfaces in cross flow, Trans. ASME 67 (1945) 643–660.
[43] Y. Peles, A. Koşar, C. Mishra, C.J. Kuo, B. Schneider, Forced convective heat transfer across a pin fin micro heat sink, Int. J. Heat Mass Transf. 48 (2005) 3615–3627, https://doi.org/10.1016/j.ijheatmasstransfer.2005.03.017.
[44] S. Feng, Y. Yan, H. Li, Z. Yang, L. Li, L. Zhang, Theoretical and numerical investigation of embedded microfluidic thermal management using gradient distribution micro pin fin arrays, Appl. Therm. Eng. 153 (2019) 748–760, https://doi.org/10.1016/j.applthermaleng.2019.03.017.
[45] H.J. Uitslag-Doolaard, F. Alcaro, F. Roelofs, X. Wang, A. Kraus, A. Brunett, J. Thomas, C. Geffray, A. Gerschenfeld, Multiscale modelling of the phénix dissymmetric test benchmark, Nucl. Eng. Des. 356 (2020) 110375.
[46] D.D. Ma, G.D. Xia, Y.F. Li, Y.T. Jia, J. Wang, Design study of micro heat sink configurations with offset zigzag channel for specific chips geometrics, Energy Convers. Manage. 127 (2016) 160–169, https://doi.org/10.1016/j.enconman.2016.09.013.